INTERNATIONAL JOURNAL OF COMPUTERS COMMUNICATIONS & CONTROL
Online ISSN 1841-9844, ISSN-L 1841-9836, Volume: 21, Issue: 5, Month: October, Year: 2026
Article Number: 7478, https://doi.org/10.15837/ijccc.2026.5.7478

CCC Publications

Algorithmic Compression Learning: A Hybrid Complexity–Deep Representation Framework for Medical Image Analysis

Soukaina Mjahed, Ouail Mjahed

Soukaina Mjahed
Faculty of Sciences Semlalia, Department of Computer Sciences
LISI Laboratory, Cadi Ayyad University
Marrakech 40000, Morocco.
s.mjahed@uca.ac.ma

Ouail Mjahed*
Faculty of Sciences and Technology, Department of Computer Sciences
L2IS Laboratory, Cadi Ayyad University
Marrakech 40000, Morocco.
*Corresponding author: ouail.mjahed@ced.uca.ma

Abstract

Understanding and quantifying structural complexity in visual data remains a fundamental challenge in pattern recognition. This work investigates the hypothesis that compression-based measures can provide a complementary structural representation that enhances deep learning models. To this end, we introduce a hybrid framework termed *Algorithmic Compression Learning with Deep Learning (ACL–DL)*, which integrates multi-scale compression-based descriptors with deep neural representations. The proposed ACL component characterizes structural irregularity and stability across spatial scales using compression-derived measures, interpreted as empirical proxies of structural organization. These descriptors are fused with semantic embeddings extracted from fine-tuned deep networks, enabling joint modeling of intrinsic structural patterns and high-level visual features. Experiments conducted on three heterogeneous medical imaging datasets (BUSI ultrasound, CBIS-DDSM mammography, and BreakHis histopathology) demonstrate that compression-based descriptors provide discriminative signals that complement deep representations. The best accuracy rates achieved by the ACL–DL hybrid framework, reported as mean + standard deviation, reached *95.63%*, *98.72%*, and *99.16%* across the three datasets, consistently improving over standalone ACL and deep learning baselines with statistically significant gains ($p < 0.05$). Beyond predictive performance, the results highlight the potential of compression-based structural descriptors as model-agnostic components that can be effectively integrated into modern representation learning pipelines.

Keywords: Algorithmic Complexity, Compression-Based Features, Representation Learning, Hybrid Deep Learning Models, Structural Pattern Analysis.

1 Introduction

Representation learning remains a central challenge in modern machine learning and pattern recognition. Deep neural networks have achieved remarkable success in extracting high-level semantic representations from complex data, particularly in computer vision and image analysis. However, their learned representations are primarily optimized for semantic discrimination and may not explicitly capture intrinsic structural irregularities present in heterogeneous textures, complex spatial organizations, or limited-data regimes. Consequently, complementary representation paradigms capable of encoding structural organization independently of purely learned semantic features have attracted increasing attention.

A promising theoretical perspective arises from Algorithmic Information Theory (AIT). In this framework, Kolmogorov complexity measures the intrinsic structural complexity of an object through the length of the shortest program capable of generating it [1, 2]. Although Kolmogorov complexity is not computable in practice, lossless compression algorithms provide heuristic approximations that can serve as practical proxies for structural regularity, rather than exact estimates of algorithmic complexity. These approximations are closely related to the Minimum Description Length (MDL) principle, which states that the most informative representation of data corresponds to its shortest description [3, 4].

From this perspective, compression length can be interpreted as an empirical indicator of structural organization: highly structured patterns can be represented more compactly, whereas irregular or heterogeneous structures require longer descriptions. Compression algorithms therefore implicitly capture statistical dependencies, redundancy, and higher-order structural organization in data. These properties have motivated the development of compression-based similarity measures such as the Normalized Compression Distance (NCD), which has been successfully applied to clustering, classification, and anomaly detection tasks [5].

Despite these theoretical motivations, compression-based structural descriptors remain relatively underexplored in modern deep learning pipelines. Most contemporary learning systems rely either on handcrafted descriptors, such as classical texture features [6], or on deep neural representations learned from large datasets [7, 8]. While deep models excel at learning semantic abstractions, they do not explicitly model intrinsic structural organization. This observation motivates the exploration of hybrid representations that combine compression-derived structural descriptors with learned deep features.

In this work, we introduce **Algorithmic Compression Learning (ACL)**, a computational framework designed to extract structural representations from compression statistics. Rather than designing a generic handcrafted descriptor, ACL is formulated as a structured representation framework that explicitly models structural organization through three coupled principles: (i) multi-scale compression complexity, (ii) dispersion-based characterization of structural variability, and (iii) perturbation-driven stability measures that quantify the robustness of compression patterns under small transformations. Together, these components provide a principled and compact characterization of algorithmic irregularities that cannot be captured by conventional statistical descriptors alone.

It is important to emphasize that ACL does not attempt to estimate Kolmogorov complexity directly. Instead, compression-based measures are interpreted as empirical proxies of structural regularity inspired by algorithmic information theory, rather than as formal estimators of algorithmic complexity.

From a representation learning perspective, ACL descriptors provide a structural embedding complementary to deep neural representations. Deep neural networks such as convolutional architectures and transformers have demonstrated strong performance in representation learning [9, 10, 11]. However, their representations are primarily optimized for semantic discrimination and do not explicitly model intrinsic structural organization. The proposed ACL–DL framework therefore does not rely on a simple feature concatenation, but establishes a unified structural–semantic representation, where compression-based descriptors encode intrinsic organization while deep networks capture high-level semantic patterns. This complementary interaction enables a more complete characterization of complex visual structures.

Although the proposed framework is general and applicable to a wide range of structured data domains, this study evaluates its effectiveness using breast imaging datasets as a representative testbed. Breast lesions exhibit complex morphological patterns and heterogeneous textural characteristics across multiple imaging modalities, including ultrasound, mammography, and histopathology [12, 13]. These properties make breast imaging a challenging benchmark for structural pattern recognition and automated diagnostic systems. The medical imaging application is therefore considered as a validation scenario to assess the relevance of the proposed representation framework.

Extensive experiments conducted on BUSI (ultrasound), CBIS-DDSM (mammography), and BreakHis (histopathology) datasets demonstrate that ACL descriptors consistently capture structural complexity patterns across heterogeneous imaging modalities. Furthermore, when combined with deep representations, the proposed hybrid ACL–DL framework improves classification performance while preserving interpretability through compression-derived structural measures.

The main contributions of this work can be summarized as follows:

- We introduce **Algorithmic Compression Learning (ACL)**, a structured representation framework that models intrinsic structural organization through compression dynamics rather than conventional handcrafted features.
- We propose a **multi-scale and stability-aware compression representation**, combining complexity, dispersion, and perturbation-based stability to capture structural heterogeneity.
- We develop a **unified structural–semantic hybrid representation (ACL–DL)**, enabling complementary integration of algorithmic complexity and deep learned features.
- We provide extensive multi-dataset validation demonstrating that ACL–DL improves robustness, interpretability, and generalization compared to both deep-only and handcrafted approaches.

Overall, this work contributes to bridging algorithmic information theory and modern representation learning by demonstrating how compression-based structural descriptors can complement deep neural representations for structural pattern analysis.

The remainder of this paper is organized as follows. Section 2 reviews related work on compression-based representations, hybrid feature learning, and deep neural architectures. Section 3 introduces the proposed Algorithmic Compression Learning (ACL) framework and its hybrid ACL–DL extension. Section 4 describes the datasets, evaluation protocol, and implementation details used in this study. Section 5 presents the experimental results together with a detailed analysis of the structural properties captured by compression-based descriptors, including robustness, ablation and statistic studies, comparison with State-of-the-Art Methods, and clinical interpretation and limitations. Finally, Section 6 summarizes the main findings and outlines potential directions for future research.

2 Related Work

Automatic analysis of complex visual patterns has been widely studied in machine learning, computer vision, and medical image analysis. Existing approaches can be broadly categorized into three main paradigms: handcrafted feature engineering, deep representation learning, and hybrid feature integration. More recently, compression-based complexity measures have emerged as an alternative perspective for characterizing structural organization in data.

2.1 Handcrafted Features and Statistical Texture Analysis

Early computer-aided diagnosis (CAD) systems relied on traditional machine learning models trained on handcrafted features extracted from medical images. Classical texture descriptors such as Gray-Level Co-occurrence Matrices (GLCM) [14], Local Binary Patterns (LBP) [15], and wavelet-based features [16] have been widely used to characterize spatial intensity patterns and tissue heterogeneity. These descriptors capture statistical dependencies between pixels and provide partial interpretability for classification tasks.

Entropy-based measures have also been investigated to quantify structural variability in imaging data. Metrics such as Shannon entropy, multiscale entropy, and Rényi entropy have been applied to capture tissue heterogeneity and disorder [17, 18]. However, these approaches rely primarily on probabilistic statistics and remain limited in capturing higher-order structural dependencies and algorithmic organization.

Although handcrafted features offer interpretability and computational efficiency, their performance is often constrained by the expressiveness of predefined descriptors and their sensitivity to imaging conditions.

2.2 Deep Representation Learning

Deep learning has significantly advanced pattern recognition and image analysis by enabling hierarchical feature learning directly from data. Convolutional neural networks (CNNs) have demonstrated strong performance across a wide range of visual recognition tasks [19, 20]. Architectures such as ResNet [21], DenseNet [22], and EfficientNet [23] have achieved state-of-the-art performance in many computer vision applications.

More recently, transformer-based architectures have extended deep representation learning by modeling long-range dependencies within visual data. Vision Transformers (ViTs) [24] and hierarchical transformer models such as Swin Transformer [25] have demonstrated strong performance in image classification and medical imaging tasks.

Despite their accuracy, deep learning models primarily learn task-driven semantic representations and do not explicitly model intrinsic structural organization. In addition, they may exhibit sensitivity to dataset bias and domain shifts across acquisition devices and institutions [26], while their internal representations remain difficult to interpret [27].

2.3 Hybrid Feature Representations

To overcome the limitations of purely handcrafted or purely learned representations, hybrid frameworks combining statistical descriptors with deep embeddings have been proposed. These approaches exploit complementary information from heterogeneous feature sources and have been shown to improve robustness and generalization performance [28]. Hybrid strategies have been successfully applied across various pattern recognition domains, including medical image analysis, texture classification, and intrusion detection [29, 30, 31].

However, most existing hybrid approaches rely on statistical or correlation-based descriptors and do not explicitly model intrinsic structural organization. As a result, their ability to capture deeper forms of structural irregularity remains limited.

2.4 Compression-Based Structural Complexity

Algorithmic Information Theory provides a conceptual framework for analyzing structural organization in data through description length. Kolmogorov complexity measures the minimal description required to generate an object [1]. Although it is not computable, lossless compression algorithms provide practical and heuristic proxies that reflect structural regularity.

Compression-based similarity measures such as the Normalized Compression Distance (NCD) have been successfully applied to clustering, classification, and pattern discovery tasks [5]. More recent studies have explored compression-based analysis to characterize structural complexity in images and networks [32].

Compared to entropy-based approaches, compression-derived measures capture broader forms of structural dependency, including redundancy and long-range organization. However, existing work has largely focused on similarity measures or standalone analysis, with limited integration into modern representation learning frameworks.

2.5 Position of This Work

The present work builds upon these complementary research directions by introducing **Algorithmic Compression Learning (ACL)**, a structured representation framework that models intrinsic structural organization through compression dynamics.

Unlike conventional handcrafted descriptors, ACL is not based on predefined statistical features but on the analysis of compression behavior across multiple scales and perturbations, enabling the characterization of structural irregularities beyond simple correlations. In contrast to purely deep learning approaches, ACL provides interpretable descriptors reflecting intrinsic structural properties rather than task-driven abstractions.

The proposed ACL–DL framework extends prior hybrid approaches by establishing a unified structural–semantic representation, where compression-based descriptors capture intrinsic organization while deep neural networks extract high-level semantic features. This integration enables a more complete and robust characterization of complex visual patterns.

While rooted in concepts from algorithmic information theory, our approach adopts a pragmatic perspective, where compression is treated as a data-driven probe of structural organization rather than a formal estimator of algorithmic complexity.

3 Methodology

This section presents the proposed *Algorithmic Compression Learning* (ACL) framework and its hybrid extension with deep learning (ACL–DL). The approach is conceptually motivated by Algorithmic Information Theory (AIT) and the Minimum Description Length (MDL) framework, which associate structural complexity with description length [1, 3].

In this work, compression-based measures are interpreted as empirical proxies of structural regularity, rather than formal estimators of Kolmogorov complexity. Although Kolmogorov complexity is not computable, lossless compression algorithms provide practical heuristics reflecting redundancy and organization in data: structured patterns are more compressible, whereas irregular patterns yield longer descriptions.

The central hypothesis is that structural irregularities induce measurable variations in compression behavior. ACL therefore models structural organization through compression dynamics across spatial scales and controlled perturbations.

3.1 Problem Formulation

Let $\mathcal{X} = \{x_i\}_{i=1}^N$ denote a dataset of images, where each image $x_i \in \mathbb{R}^{H\times W}$ is associated with a label $y_i \in \mathcal{Y}$. The objective is to learn a prediction function

$$f : x_i \mapsto y_i, \tag{1}$$

using compression-derived structural representations, optionally combined with deep semantic features. Figure 1 illustrates the proposed ACL–DL framework.

3.2 ACL Representation

The ACL framework extracts structural representations through four stages:
(i) multi-scale decomposition,
(ii) compression-based complexity estimation,
(iii) perturbation-based stability analysis, and
(iv) feature aggregation.

Each image is decomposed into patches across dyadic scales $\mathcal{S} = \{16, 32, 64\}$:

$$\mathcal{P}_i = \bigcup_{s\in\mathcal{S}} \{p_{i,j}^{(s)}\}. \tag{2}$$

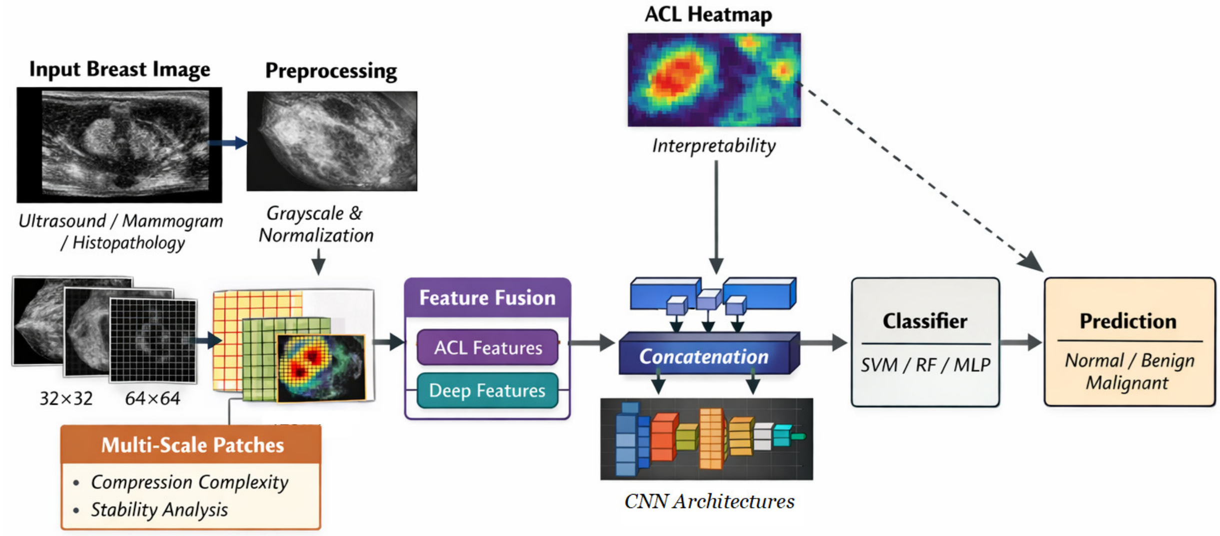

Figure 1: Overview of the proposed ACL–DL framework. Multi-scale compression descriptors capture structural complexity, while deep networks extract semantic representations.

Multi-scale analysis is essential to capture hierarchical structure: fine scales encode local textures, while coarser scales capture global organization [15, 16].

The selected scales (16, 32, 64) correspond to fine, mesoscopic, and coarse structural levels. This choice reflects a trade-off between spatial resolution and statistical reliability, as larger patches reduce sample size while smaller patches increase sensitivity to noise.

Each patch $p_{i,j}^{(s)}$ is quantized into a symbolic sequence:

$$q_{i,j}^{(s)} = Q(p_{i,j}^{(s)}), \tag{3}$$

where the mapping $Q(: \mathbb{R} \to \Sigma)$ assigns pixel intensities to a discrete alphabet Σ, enabling sequence-based compression.

Compression complexity is estimated using a universal compressor $C(\cdot)$ (as LZMA, a variant of the Lempel–Ziv family of universal compression algorithms, adopted in this work):

$$K_{i,j}^{(s)} = \frac{C(q_{i,j}^{(s)})}{|q_{i,j}^{(s)}|}. \tag{4}$$

where $|q_{i,j}^{(s)}|$ denotes the uncompressed sequence length. Higher values indicate lower compressibility and therefore greater structural irregularity.

To capture robustness, patches are subjected to perturbations $T_t \in \mathcal{T}$:

$$\tilde{p}_{i,j}^{(s,t)} = T_t(p_{i,j}^{(s)}). \tag{5}$$

Compression stability is defined as the variance of compression estimates across perturbations:

$$S_{i,j}^{(s)} = \mathrm{Var}_t(K_{i,j}^{(s,t)}). \tag{6}$$

This stability term reflects sensitivity to structural perturbations, with irregular patterns exhibiting higher variability.

Patch-level measures are aggregated into image-level descriptors:

$$\mu^{(s)} = \mathbb{E}[K^{(s)}], \quad \sigma^{(s)} = \mathrm{Std}[K^{(s)}], \quad \bar{S}^{(s)} = \mathbb{E}[S^{(s)}]. \tag{7}$$

The final ACL representation is:

$$\phi_{ACL} = [\mu^{(16)}, \sigma^{(16)}, \bar{S}^{(16)}, \mu^{(32)}, \sigma^{(32)}, \bar{S}^{(32)}, \mu^{(64)}, \sigma^{(64)}, \bar{S}^{(64)}]. \tag{8}$$

The proposed descriptor is intentionally minimal and designed to capture complementary aspects of structural organization.

The mean reflects average structural irregularity, the standard deviation captures spatial heterogeneity, and the stability term quantifies sensitivity to perturbations.

Higher-order statistics were explored in preliminary experiments but did not provide consistent improvements and were therefore not retained to preserve robustness and interpretability.

Fig. 2 details the ACL feature construction process.

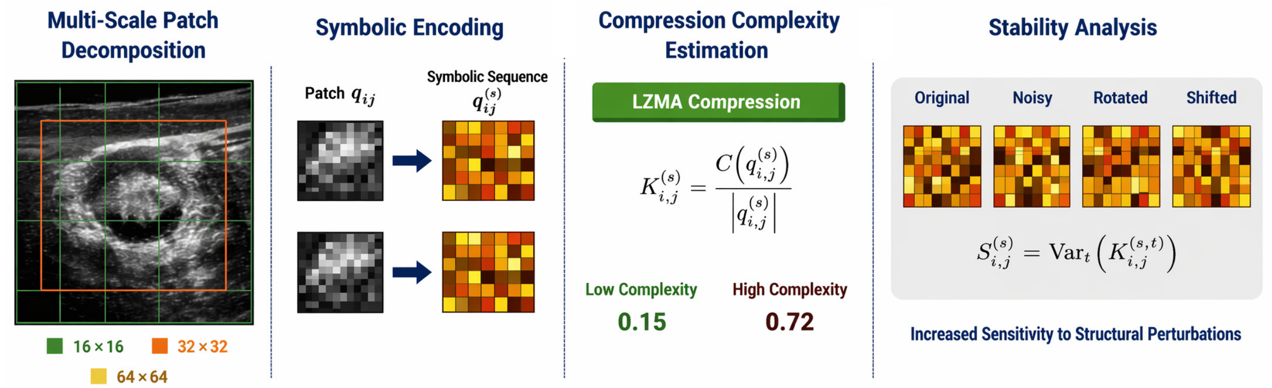

Figure 2: Overview of the ACL feature construction process, comprising multi-scale decomposition of patches, followed by a compression-based complexity estimate and a stability analysis.

3.3 Hybrid Structural–Semantic Representation

In the ACL–DL configuration, deep features are extracted from pretrained models (e.g., ResNet [21], DenseNet [22], ViT [24, 33]).

$$\mathbf{f}_{DL,i} = \phi_{DL}(x_i). \tag{9}$$

ACL and deep representations encode complementary information: compression captures intrinsic structural organization, while deep networks capture semantic abstractions.

The hybrid representation is defined as:

$$\mathbf{f}_{Hybrid,i} = [\mathbf{f}_{DL,i} \| \mathbf{f}_{ACL,i}]. \tag{10}$$

This formulation establishes a unified structural–semantic representation, rather than a simple feature augmentation.

3.4 Classification and Algorithmic Summary

Predictions are obtained as:

$$\hat{y}_i = \begin{cases} g(\mathbf{f}_{ACL,i}), & \text{ACL only} \\ g(\mathbf{f}_{Hybrid,i}), & \text{ACL–DL} \end{cases} \tag{11}$$

where $g(\cdot)$ is a classifier (SVM, Multi-Layer Perceptron (MLP)).

The ACL-DL pipeline is summarized in Algorithm 1.

The framework provides:

(i) a compression-based structural representation,

(ii) robustness through perturbation stability, and

(iii) compatibility with deep representation learning.

Algorithm 1: Unified ACL / ACL–DL Diagnostic Pipeline

Input: Image x_i, scales $\mathcal{S}$, compressor C, perturbations $\mathcal{T}$, hybrid flag h
Output: Predicted label $\hat{y}_i$

Preprocess x_i (grayscale + normalization);
Initialize $\Phi_i \leftarrow \emptyset$;
foreach *scale* s *in* $\mathcal{S}$ **do**
    Extract patches $\{p_{i,j}^{(s)}\}$;
    foreach *patch* $p_{i,j}^{(s)}$ **do**
        Quantize: $q_{i,j}^{(s)} \leftarrow Q(p_{i,j}^{(s)})$;
        Compute complexity: $K_{i,j}^{(s)} \leftarrow \frac{C(q_{i,j}^{(s)})}{|q_{i,j}^{(s)}|}$;
        Compute stability: $S_{i,j}^{(s)} \leftarrow \mathrm{Var}_{T \in \mathcal{T}}(K(T(p_{i,j}^{(s)})))$;
    Aggregate $\mu^{(s)}, \sigma^{(s)}, \bar{S}^{(s)}$;
    Append $[\mu^{(s)}, \sigma^{(s)}, \bar{S}^{(s)}]$ to Φ_i;
if $h = 1$ **then**
    $\mathbf{F}_{DL} \leftarrow \mathrm{Backbone}(x_i)$;
    $\hat{y}_i \leftarrow g_{Hybrid}([\mathbf{F}_{DL}, \Phi_i])$;
else
    $\hat{y}_i \leftarrow g_{ACL}(\Phi_i)$;
return $\hat{y}_i$

4 Experimental Setup

This section describes the experimental design used to evaluate the proposed Algorithmic Compression Learning (ACL) framework and its hybrid extension (ACL–DL). The evaluation aims to assess (i) the discriminative power of compression-based descriptors, (ii) the contribution of multi-scale modeling, and (iii) the complementarity between structural and deep representations.

4.1 Datasets

Experiments are conducted on three publicly available breast imaging datasets covering complementary modalities.

BUSI (Breast Ultrasound Images) [34]: 780 images categorized into normal (133), benign (437), and malignant (210).

CBIS-DDSM (Mammography) [35]: The Curated Breast Imaging Subset of DDSM provides digitized mammograms with pathology-verified labels and annotated regions of interest (ROIs).

BreakHis (Histopathology) [36]: 9,109 microscopic images acquired at multiple magnifications (40×–400×), including 2,480 benign and 5,429 malignant samples from multiple patients.

4.2 Preprocessing and ROI Handling

A unified preprocessing pipeline is applied across all datasets, including grayscale conversion, intensity normalization, resizing to 224×224 for deep models, and multi-scale patch decomposition ($s \in \{16, 32, 64\}$). Prior to compression-based analysis, patches are quantized using an adaptive uniform scheme.

ROI handling is standardized to ensure consistency across datasets. For CBIS-DDSM, feature extraction is performed on annotated lesion-centered regions of interest (ROIs), which are resized to a fixed resolution. For BUSI and BreakHis, images are inherently lesion-focused and are therefore treated as effective ROIs without additional cropping.

Importantly, both ACL descriptors and deep features are extracted from the same spatial regions in all cases, ensuring that the learned representations reflect intrinsic tissue structure rather than background variability.

4.3 Baseline Methods

The proposed framework is compared with representative approaches:

- **Deep learning:** ResNet-50, DenseNet-121, ViT-B/16,
- **ACL-only:** compression descriptors with Support Vector Machine (SVM) or Random Forest (RF),
- **Handcrafted:** GLCM-SVM, LBP-RF,
- **Entropy-based:** Shannon and multiscale entropy - SVM.

All methods are evaluated under identical conditions to ensure fairness. Hyperparameters for classical models are tuned within training folds.

4.4 Experimental Protocol

All methods are evaluated under a unified and reproducible protocol with identical data splits, preprocessing, and training settings.

A strict patient-level 10-fold cross-validation strategy is employed, where all samples belonging to the same patient are assigned to a single fold prior to any preprocessing or feature extraction. This guarantees complete separation between training and testing data and eliminates any risk of data leakage.

For BreakHis, patient identifiers are used to group all images across different magnification levels within the same fold. For CBIS-DDSM, ROI samples are grouped according to case identifiers, ensuring that all regions from the same patient study are assigned to a single fold. Similar precautions are applied to other datasets whenever metadata is available.

All preprocessing operations are computed exclusively on training data and then applied to test samples. Deep models are initialized with ImageNet pretrained weights and fine-tuned using identical training settings (Adam optimizer, learning rate 10^{-4}, batch size 32, 50 epochs). Handcrafted descriptors are evaluated using classifiers tuned via grid search within training folds only, and hyperparameters for all methods are optimized under the same validation strategy.

The hybrid ACL–DL models rely on a simple feature concatenation scheme, without additional tuning complexity, ensuring that performance gains are not due to increased optimization effort.

Overall, this protocol enforces strict experimental fairness and provides a realistic evaluation of generalization across patients rather than memorization of correlated samples.

4.5 Evaluation Metrics and Statistical Analysis

Performance is evaluated using Accuracy (Acc), Recall (R), F_1-score, False Alarm Rate (FAR), and AUC.

Statistical analysis is conducted across cross-validation folds. Normality and homogeneity are verified using Shapiro–Wilk and Levene tests. Inter-group differences are assessed using one-way ANOVA (F_A):

$$F_A = \frac{V_b}{V_w}. \tag{12}$$

where V_b and V_w denote between-class and within-class variances.

Paired comparisons are performed using Student's t-test and Wilcoxon signed-rank test:

$$t = \frac{\bar{d}}{s_d/\sqrt{n}}, \quad Z = \frac{W - \mu_W}{\sigma_W}. \tag{13}$$

where $\bar{d}$ denotes the mean difference and s_d its standard deviation, n is the number of paired samples. W is the Wilcoxon statistic, μ_W, σ_W its expected mean and standard deviation.

Significance is established at $p < 0.05$.

4.6 Implementation Details

Experiments are implemented using Python 3.10, PyTorch 2.2, and Scikit-learn. Compression is performed using the `lzma` library.

Experiments are executed on an NVIDIA RTX A6000 GPU. ACL feature extraction is lightweight and performed on CPU, while GPU resources are used for deep model training.

5 Results and Discussion

This section provides a comprehensive analysis of the experimental results obtained with the proposed *Algorithmic Compression Learning* (ACL) framework and its hybrid extension with deep learning (ACL–DL). The focus is placed not only on predictive performance, but also on understanding the underlying properties and contributions of compression-based algorithmic complexity descriptors.

Rather than limiting the discussion to accuracy metrics, this section aims to address three fundamental research questions: (i) whether compression-based descriptors are capable of capturing intrinsic structural differences between benign and malignant tissues, (ii) how algorithmic complexity compares as a standalone representation against conventional handcrafted features and deep neural embeddings, and (iii) whether the hybrid ACL–DL formulation provides complementary information that enhances robustness and diagnostic performance.

To systematically address these questions, the analysis is structured into six components: (i) an examination of the intrinsic behavior of ACL descriptors, (ii) a quantitative evaluation of classification performance, (iii) an ablation study to assess the contribution of individual components, (iv) statistical validation of the observed performance gains, (v) a comparison with recent state-of-the-art approaches, and (vi) a discussion of clinical relevance and limitations.

All reported results are obtained under a strict patient-level evaluation protocol, ensuring that performance reflects generalization across patients rather than memorization of subject-specific patterns.

5.1 Intrinsic Behavior of ACL Descriptors

We first investigate whether ACL descriptors encode meaningful structural information across classes. Features are computed at scales $s \in \{16, 32, 64\}$ and include mean complexity $\mu^{(s)}$, dispersion $\sigma^{(s)}$, and stability $\bar{S}^{(s)}$.

Results on the BUSI dataset (Table 1) reveal consistent and interpretable trends. Malignant lesions exhibit higher compression complexity and dispersion, together with lower stability, compared to benign and normal tissues. These observations are consistent with the known structural properties of malignancy, which is characterized by architectural disorder and heterogeneity.

Table 1: Multi-scale statistical characterization of ACL descriptors on the BUSI dataset with one-way ANOVA results (mean ± std).

Scale	**Class**	$\mu^{(s)}$	$\sigma^{(s)}$	$\bar{S}^{(s)}$	F_A	p-value	Partial η^2
16	Normal	0.412 ± 0.028	0.083 ± 0.011	0.798 ± 0.024	6.84	0.0012	0.017
16	Benign	0.436 ± 0.031	0.097 ± 0.013	0.777 ± 0.026			
16	Malignant	0.471 ± 0.034	0.118 ± 0.016	0.749 ± 0.029			
32	Normal	0.458 ± 0.030	0.091 ± 0.012	0.801 ± 0.022	18.42	< 0.001	0.045
32	Benign	0.497 ± 0.033	0.113 ± 0.014	0.773 ± 0.025			
32	Malignant	0.548 ± 0.037	0.149 ± 0.018	0.728 ± 0.031			
64	Normal	0.489 ± 0.032	0.102 ± 0.014	0.791 ± 0.021	9.76	< 0.001	0.024
64	Benign	0.522 ± 0.035	0.121 ± 0.016	0.768 ± 0.027			
64	Malignant	0.561 ± 0.039	0.138 ± 0.019	0.754 ± 0.030			

One-way ANOVA confirms statistically significant inter-class differences ($p < 0.05$) across all descriptors and scales. The most pronounced separation is observed at the intermediate scale ($s = 32$), suggesting that mesoscopic structural organization provides the most discriminative information. Fine scales ($s = 16$) primarily capture local texture variations, while coarse scales ($s = 64$) reflect global morphological patterns.

Figure 3 further illustrates class separability through two-dimensional projections of selected ACL components. Clear cluster structures are observed, indicating that compression-based descriptors provide intrinsically discriminative representations.

Similar trends are consistently observed on CBIS-DDSM and BreakHis, despite differences in imaging modality. Malignant samples systematically exhibit higher complexity, dispersion, and instability, confirming that ACL captures a modality-independent structural signal associated with tissue heterogeneity.

Overall, these results demonstrate that compression-based descriptors encode meaningful structural information prior to classification, supporting their role as intrinsic representations of tissue organization.

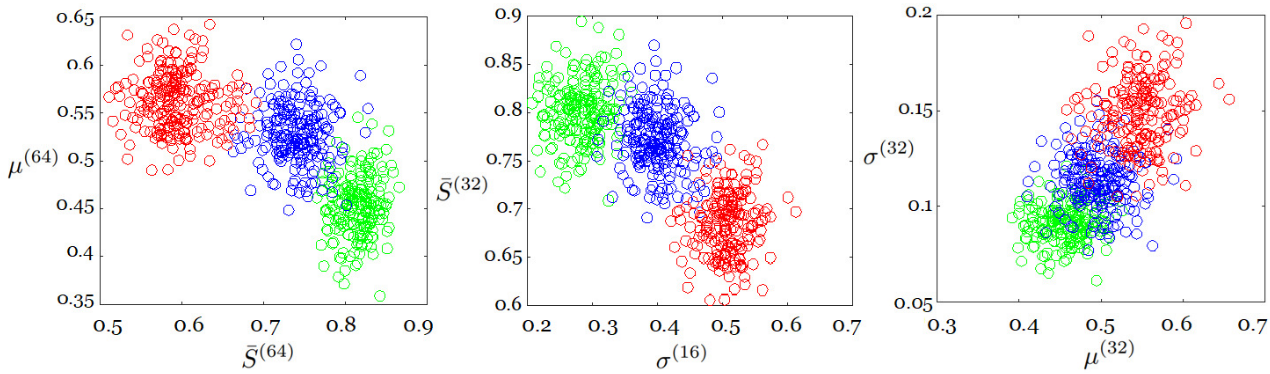

Figure 3: Two-dimensional projections of selected ACL components for BUSI Dataset, representing, $\mu^{(64)}$ vs. $\bar{S}^{(64)}$, $\bar{S}^{(32)}$ vs. $\sigma^{(16)}$, and $\sigma^{(32)}$ vs. $\mu^{(32)}$ (normal in green, benign in blue, malignant in red).

5.2 Quantitative Classification Performance

Table 2 summarizes the classification performance of handcrafted features, standalone ACL descriptors, deep neural networks, and the proposed hybrid ACL–DL framework.

The proposed method consistently achieves strong performance across datasets, with improvements observed for both predictive accuracy and robustness. Three key observations emerge.

ACL versus handcrafted features: ACL descriptors consistently outperform classical texture-based approaches (GLCM, LBP, entropy) across all datasets. On BUSI, ACL achieves an F_1-score of 90.16%, compared to 82.23% for GLCM-SVM. Similar improvements are observed on CBIS-DDSM (91.68% vs. 81.39%) and BreakHis (93.49% vs. 84.51%).

These results highlight the limitations of conventional second-order statistics, which primarily capture local correlations. In contrast, compression-based descriptors encode higher-order structural dependencies and broader spatial organization.

ACL versus deep learning: Deep models such as ResNet-50 and DenseNet-121 achieve strong performance due to hierarchical feature learning. However, standalone ACL remains competitive despite its low-dimensional and data-efficient nature. For example, on CBIS-DDSM, ACL reaches 91.68% F_1, compared to 94.89% for ResNet-50.

This suggests that compression-based structural descriptors provide discriminative information that does not rely on large-scale training data or high model capacity.

Impact of hybrid ACL–DL: The hybrid framework consistently yields the best performance. On BUSI, ACL–ResNet-50 improves F_1 from 93.32% to 94.35% and reduces FAR from 4.79% to 3.71%. On CBIS-DDSM, F_1 increases from 94.89% to 97.34%, with FAR reduced from 4.26% to 2.57%. On

BreakHis, ACL–DenseNet-121 improves F_1 from 96.41% to 98.68%, while reducing FAR from 2.44% to 0.71%.

These improvements indicate that ACL and deep representations provide complementary information: deep networks model semantic morphology, whereas ACL encodes intrinsic structural irregularity. Their combination therefore produces a richer and more robust representation.

All results are obtained under a strict patient-level cross-validation protocol, supporting generalization across subjects rather than memorization of correlated samples. Nevertheless, performance should be interpreted in the context of curated datasets and ROI-based evaluation, which may lead to optimistic estimates compared with real-world clinical settings.

Overall, the hybrid framework improves mean accuracy by approximately +1.71%, +3.45%, and +1.96% over the corresponding deep baselines on BUSI, CBIS-DDSM, and BreakHis, respectively, while consistently reducing FAR. These results support the effectiveness of structural–semantic feature integration.

Table 2: Comparative Performance of Hybrid ACL – DL and Baselines on Breast Cancer Datasets (mean ± std, 10-fold CV)

Method	***Acc*** (%)	***R*** (%)	F_1 (%)	***FAR*** (%)	***AUC***
			BUSI		
Entropy - SVM	78.61 ± 2.02	75.81 ± 1.26	77.41 ± 2.12	19.01 ± 0.41	0.793 ± 0.011
LBP - RF	81.23 ± 1.81	78.56 ± 1.31	80.10 ± 1.59	16.15 ± 0.56	0.812 ± 0.022
GLCM - SVM	83.51 ± 1.62	80.34 ± 1.23	82.23 ± 1.27	14.21 ± 0.31	0.838 ± 0.011
ACL Only	90.81 ± 1.23	89.25 ± 0.91	90.16 ± 1.34	7.61 ± 0.32	0.904 ± 0.031
ResNet-50	92.92 ± 1.01	92.61 ± 1.34	93.32 ± 1.21	4.79 ± 0.19	0.936 ± 0.022
ACL-ResNet-50	**94.63 ± 1.00**	**94.33 ± 0.92**	**94.35 ± 0.90**	**3.71 ± 0.19**	**0.945 ± 0.021**
			CBIS-DDSM		
Entropy - SVM	77.89 ± 2.08	74.61 ± 1.72	76.51 ± 2.01	19.87 ± 0.31	0.793 ± 0.019
LBP - RF	80.41 ± 1.85	77.78 ± 1.69	79.19 ± 1.77	17.39 ± 0.22	0.815 ± 0.018
GLCM - SVM	82.67 ± 1.67	79.91 ± 1.51	81.39 ± 1.54	15.02 ± 0.21	0.847 ± 0.014
ACL Only	92.28 ± 1.16	91.76 ± 1.18	91.68 ± 1.24	7.09 ± 0.12	0.945 ± 0.013
ResNet-50	94.49 ± 1.01	94.09 ± 1.08	94.89 ± 1.09	4.26 ± 0.11	0.957 ± 0.013
ACL-ResNet-50	**97.94 ± 0.78**	**97.19 ± 0.91**	**97.34 ± 0.85**	**2.57 ± 0.09**	**0.971 ± 0.010**
			BreakHis		
Entropy - SVM	80.49 ± 1.89	77.91 ± 2.01	79.61 ± 1.78	17.23 ± 0.32	0.811 ± 0.029
LBP - RF	83.77 ± 1.58	81.32 ± 1.88	82.69 ± 1.51	14.01 ± 0.23	0.845 ± 0.020
GLCM - SVM	85.59 ± 1.51	83.02 ± 1.68	84.51 ± 1.34	12.24 ± 0.24	0.867 ± 0.014
ACL Only	94.01 ± 1.01	92.78 ± 1.53	93.49 ± 1.11	4.88 ± 0.19	0.953 ± 0.015
DenseNet-121	96.78 ± 0.81	95.67 ± 1.45	96.41 ± 0.87	2.44 ± 0.18	0.972 ± 0.009
ACL-DenseNet-121	**98.74 ± 0.42**	**98.85 ± 0.86**	**98.68 ± 0.75**	**0.71 ± 0.09**	**0.989 ± 0.006**

Training dynamics: Figure 4 shows the evolution of classification performance during training. The hybrid ACL–ResNet-50 model converges faster and stabilizes earlier than the deep network alone. This behavior suggests that ACL descriptors provide structural priors that facilitate optimization by guiding the learning process toward informative regions of the feature space. In contrast, classical descriptors produce static feature spaces and therefore show no training dynamics.

ROC analysis: Receiver Operating Characteristic curves further confirm the robustness of the hybrid framework (Fig. 5). ACL descriptors alone already achieve strong AUC values (0.904 on BUSI, 0.945 on CBIS-DDSM, and 0.953 on BreakHis), indicating intrinsic class separability. Hybridization further improves these margins, reaching an AUC of 0.989 on BreakHis.

This demonstrates that the hybrid representation does not only improve classification accuracy but also strengthens ranking performance across decision thresholds.

Beyond raw performance, the consistency of results across datasets and folds supports the robustness of the proposed framework.

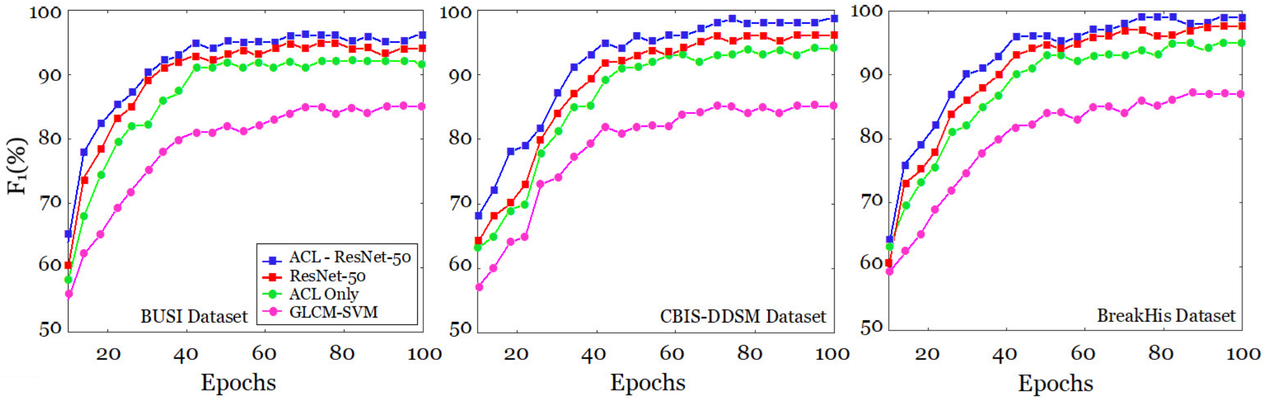

Figure 4: F_1-score evolution during training for deep and hybrid ACL–DL models, illustrating faster convergence and improved stability of the hybrid framework.

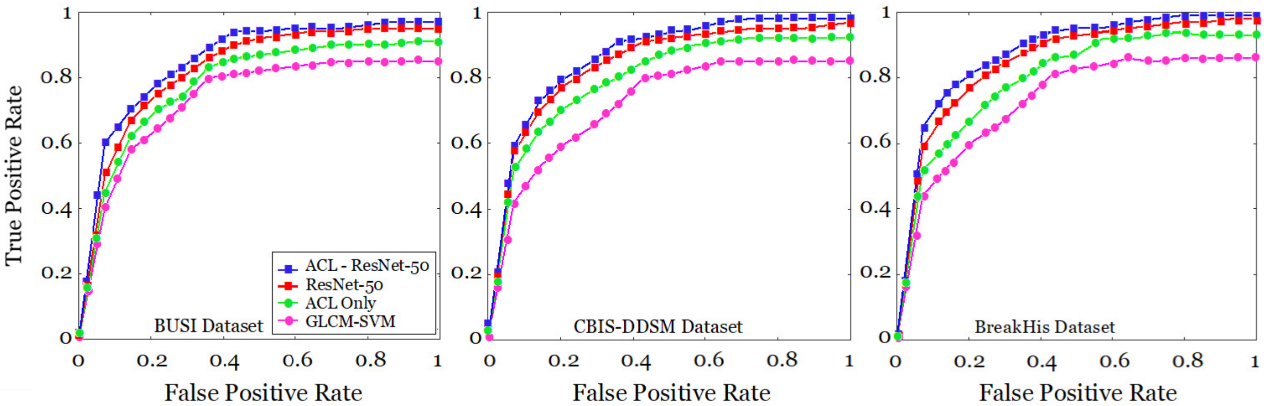

Figure 5: Receiver Operating Characteristic (ROC) curves comparing standalone ACL, deep learning backbones, and the proposed hybrid ACL–DL framework.

5.3 Ablation Study

We evaluate the contribution of each component of the ACL–DL framework using 10-fold cross-validation. For clarity, detailed analysis is presented on the BUSI dataset, while similar trends are observed on CBIS-DDSM and BreakHis. Table 3 shows that ACL descriptors alone provide competitive performance, further improved by multi-scale analysis. Deep models achieve strong baselines, while the hybrid ACL–DL consistently yields the best results, confirming the complementarity between algorithmic complexity and deep representations.

Impact of model components: On BUSI, multi-scale ACL outperforms single-scale descriptors, highlighting the importance of capturing both local and global structures. Removing the stability term slightly degrades performance, confirming its contribution to robustness. The full ACL–DL model achieves the highest accuracy and F_1.

Compression algorithms: Results (Table 4) show that LZMA consistently outperforms Brotli and BWT–Huffman, due to its ability to capture long-range dependencies.

Patch scale analysis: Table 5 confirms that multi-scale decomposition outperforms single-scale settings, demonstrating the importance of modeling both micro-textures and global tissue structure.

Feature fusion: As shown in Table 6, hybrid ACL–DL features outperform standalone ACL or deep features, confirming their complementarity.

Classifier selection: Among evaluated classifiers (Table 7), SVM provides the best performance and stability, suggesting that the hybrid feature space is largely linearly separable.

Table 3: Ablation study of the proposed Hybrid ACL+DL framework (mean ± std, 10-fold CV)

Configuration	***Acc*** **(%)**	***R*** **(%)**	F_1 **(%)**
	BUSI		
DL only (ResNet-50)	92.92 ± 1.01	92.61 ± 1.34	93.32 ± 1.21
ACL only (single-scale)	87.84 ± 1.35	86.72 ± 1.28	87.43 ± 1.30
ACL only (multi-scale)	89.96 ± 1.27	88.94 ± 1.19	89.62 ± 1.22
ACL - DL (w/o stability)	93.78 ± 0.94	93.41 ± 1.02	93.56 ± 0.98
ACL - DL (full model)	**94.63 ± 1.00**	**94.33 ± 0.92**	**94.35 ± 0.90**

Table 4: Impact of the compression algorithm used in ACL (mean ± std, 10-fold CV).

Compressor	***Acc*** **(%)**	***R*** **(%)**	F_1 **(%)**
	BUSI		
BWT–Huffman	86.92 ± 1.48	85.74 ± 1.39	86.41 ± 1.42
Brotli	88.61 ± 1.34	87.52 ± 1.28	88.13 ± 1.30
LZMA	**89.96 ± 1.27**	**88.94 ± 1.19**	**89.62 ± 1.22**

Table 5: Impact of patch scale on ACL performance using LZMA compression (mean ± std, 10-fold CV).

Patch Scale	***Acc*** **(%)**	***R*** **(%)**	F_1 **(%)**
	BUSI		
16×16	87.02 ± 1.46	85.93 ± 1.38	86.61 ± 1.41
32×32	88.45 ± 1.36	87.52 ± 1.29	88.03 ± 1.32
64×64	87.84 ± 1.39	86.71 ± 1.34	87.32 ± 1.36
Multi-scale	**89.96 ± 1.27**	**88.94 ± 1.19**	**89.62 ± 1.22**

Table 6: Impact of feature fusion on classification performance (mean ± std, 10-fold CV).

Feature Set	***Acc*** **(%)**	***R*** **(%)**	F_1 **(%)**
	BUSI		
Deep features only	92.92 ± 1.01	92.61 ± 1.34	93.32 ± 1.21
ACL features only	89.96 ± 1.27	88.94 ± 1.19	89.62 ± 1.22
ACL - DL (Hybrid)	**93.78 ± 0.94**	**93.41 ± 1.02**	**94.35 ± 0.90**

Table 7: Impact of classifier choice on ACL–DL performance (mean ± std, 10-fold CV).

Classifier	***Acc*** **(%)**	***R*** **(%)**	F_1 **(%)**
	BUSI		
RF	92.61 ± 1.02	92.14 ± 1.15	92.31 ± 1.07
MLP	93.24 ± 0.98	92.87 ± 1.08	93.01 ± 1.00
SVM	**93.78 ± 0.94**	**93.41 ± 1.02**	**93.56 ± 0.98**

Similar improvements are consistently observed on CBIS-DDSM and BreakHis, confirming the generality of these findings. Overall, the ablation study validates that performance gains arise from the synergy between multi-scale analysis, compression-based descriptors, stability modeling, and deep feature fusion.

The ablation results confirm that each component of the ACL descriptor contributes to performance: removing multi-scale information, dispersion, or stability leads to consistent degradation, validating the necessity of the proposed design.

5.4 Statistical Significance Analysis

To ensure that the observed performance improvements are not due to random variations across cross-validation folds, statistical hypothesis testing was conducted on fold-wise results.

Paired comparisons between methods were performed using Student's t-test under the assumption of normality, and the Wilcoxon signed-rank test as a non-parametric alternative. These tests were applied to performance differences between the proposed ACL–DL framework and its ablated variants.

In addition, one-way ANOVA was used to assess inter-class differences in multi-scale ACL descriptors. Prior to ANOVA, normality and homogeneity of variances were verified using the Shapiro–Wilk and Levene tests, respectively.

Table 8 summarizes the statistical comparison results. All improvements achieved by the hybrid ACL–DL framework are statistically significant across datasets ($p < 0.01$) for both parametric and non-parametric tests. Moreover, Cohen's d values indicate large effect sizes, confirming that the observed gains are not only statistically significant but also practically meaningful.

The agreement between t-test and Wilcoxon results further supports the robustness and consistency of the proposed framework across cross-validation folds.

Although the number of statistical comparisons is limited, the potential risk of Type I error inflation is taken into account when interpreting the results. The Holm–Bonferroni correction is applied to control the family-wise error rate, under which the results remain significant. The consistency of results across parametric and non-parametric tests, together with large effect sizes, supports the robustness of the observed improvements.

The extended statistical analysis confirms that improvements are consistent across all baselines, with large effect sizes ($d > 1$), supporting both statistical and practical significance.

Table 8: Statistical significance analysis comparing ACL–DL with baseline and ablated models (10-fold cross-validation)

Comparison	***Paired t-test***		***Wilcoxon test***				***Effect***
	t	p_t	***W***	***Z***	p_W	***Sig.***	***Cohen's*** d
BUSI							
ACL–DL vs DL only	4.72	1.8×10^{-3}	15	-3.12	1.8×10^{-3}	Yes	1.49
ACL–DL vs ACL only	5.11	9.6×10^{-4}	13	-3.29	9.9×10^{-4}	Yes	1.62
ACL only vs GLCM–SVM	3.85	3.1×10^{-3}	18	-2.87	4.1×10^{-3}	Yes	1.22
ACL–DL vs GLCM–SVM	6.12	3.2×10^{-4}	8	-3.85	1.2×10^{-4}	Yes	1.94
CBIS-DDSM							
ACL–DL vs DL only	4.35	2.4×10^{-3}	16	-3.05	2.3×10^{-3}	Yes	1.38
ACL–DL vs ACL only	4.89	1.2×10^{-3}	14	-3.18	1.5×10^{-3}	Yes	1.55
ACL only vs GLCM–SVM	3.62	4.5×10^{-3}	19	-2.75	5.8×10^{-3}	Yes	1.15
ACL–DL vs GLCM–SVM	5.74	4.1×10^{-4}	9	-3.68	2.3×10^{-4}	Yes	1.81
BreakHis							
ACL–DL vs DL only	5.26	7.9×10^{-4}	12	-3.41	6.5×10^{-4}	Yes	1.66
ACL–DL vs ACL only	5.73	4.5×10^{-4}	10	-3.57	3.6×10^{-4}	Yes	1.81
ACL only vs GLCM–SVM	4.02	2.6×10^{-3}	17	-2.95	3.2×10^{-3}	Yes	1.27
ACL–DL vs GLCM–SVM	6.45	2.1×10^{-4}	7	-3.92	9.0×10^{-5}	Yes	2.04

5.5 Comparison with State-of-the-Art Methods

Table 9 compares the proposed ACL–DL framework with recent machine learning and deep learning approaches reported in the literature.

Comparisons with previously published results should be interpreted with caution, as differences in data splits, preprocessing, ROI selection, and evaluation protocols limit direct comparability. Therefore, these results should be considered indicative rather than strictly comparable.

Despite these differences, the proposed method maintains consistently strong performance across datasets, achieving peak accuracies, expressed as mean + standard deviation, of 95.63%, 98.72%, and 99.16% on BUSI, CBIS-DDSM, and BreakHis, respectively.

The improvements are particularly notable on heterogeneous datasets such as BreakHis, suggesting that compression-based structural descriptors capture variability not fully modeled by conventional deep features. This highlights the complementary nature of structural (ACL) and semantic (deep) representations. Overall, while results are obtained under controlled experimental conditions, the consistency of performance gains across datasets supports the effectiveness and robustness of the proposed hybrid framework.

Table 9: Comparison with recent ML and DL approaches on BUSI, CBIS-DDSM, and BreakHis datasets

Reference	Method	*Acc* (%)	*R* (%)	F_1 (%)
	BUSI Dataset			
[37]	DNBCD	90.90	90.90	90.91
[38]	ProtoNet-ResNet50	88.90	–	–
[39]	ViT-B32	86.70	–	–
[40]	HAU-Net	83.11	–	–
This work	**ACL–ResNet-50**	**95.63**	**95.25**	**95.25**
	CBIS-DDSM Dataset			
[41]	CNN-SGD	96.00	95.00	–
[42]	CNN (NasNet, MobileNet)	91.20	92.31	91.76
[43]	DNN-WOA	93.80	93.75	93.77
[44]	IMPA-ResNet50	98.32	96.61	97.65
This work	**ACL–ResNet-50**	**98.72**	**98.10**	**98.19**
	BreakHis Dataset			
[45]	CNN	91.60	–	–
[46]	ResRFSAM-LSTM (200×)	98.01	–	–
[47]	IDSNet (200×)	93.00	–	–
[48]	DenseNet (200×)	95.87	–	–
This work	**ACL–DenseNet-121**	**99.16**	**99.71**	**99.43**

5.6 Clinical Interpretation and Limitations

From an interpretability perspective, ACL descriptors provide a direct quantification of structural irregularity derived from compression behavior. Unlike post-hoc explanation techniques, these descriptors are intrinsically linked to the underlying organization of image patterns, offering a transparent representation of tissue heterogeneity.

The observed performance gains can be attributed to the complementary nature of the representation: compression-based descriptors capture intrinsic structural variability, while deep features encode semantic information. This structural–semantic interaction enables a more comprehensive characterization of complex tissue patterns.

Despite these promising results, several limitations should be noted.

First, compression-based measures depend on the selected algorithm and should be interpreted as empirical indicators rather than exact approximations of algorithmic complexity.

Second, the current framework relies on predefined patch scales rather than adaptive multi-scale selection. In addition, the descriptor may be sensitive to image resolution, quantization parameters, and lesion size. Although normalization and multi-scale aggregation mitigate these effects, further investigation is required to assess robustness under varying acquisition conditions.

Third, the evaluation is conducted on curated datasets using lesion-centered ROIs, which simplifies the task compared to full-image clinical scenarios. In practice, automatic lesion localization would be required prior to classification.

Fourth, statistical analyses are performed on cross-validation folds, which are not strictly independent. Consequently, reported p-values should be interpreted as indicative rather than definitive measures of significance.

Finally, although patient-level cross-validation mitigates data leakage, the limited number of patients and the curated nature of certain datasets (e.g., BreakHis) may lead to optimistic estimates of generalization.

Future work will address these limitations by exploring adaptive multi-scale strategies, multi-compressor ensembles, and tighter integration of compression-based representations within neural architectures. The incorporation of automatic lesion localization and prospective multi-center validation will also be essential to assess real-world clinical robustness.

6 Conclusion and Future Work

This work investigated whether compression-based approximations of algorithmic complexity can provide meaningful structural representations to complement deep neural features. We introduced the *Algorithmic Compression Learning (ACL)* framework and its hybrid extension (ACL–DL), which combines compression-derived descriptors with learned representations.

Experimental results on BUSI, CBIS-DDSM, and BreakHis demonstrate that ACL descriptors capture discriminative structural information across modalities. Standalone ACL achieves strong performance, with average F_1-scores of 90.16%, 91.68%, and 93.49%, respectively, outperforming classical handcrafted descriptors.

When integrated with deep models, the ACL–DL framework consistently improves performance. On BUSI, ACL–ResNet50 achieves 94.63% accuracy and 94.35% F_1, compared to 92.92% and 93.32% for ResNet50 alone. On CBIS-DDSM, accuracy increases from 94.49% to 97.94%, while F_1 improves from 94.89% to 97.34%. On BreakHis, ACL–DenseNet121 reaches 98.74% accuracy and 98.68% F_1, outperforming DenseNet-121 (96.78% accuracy and 96.41% F_1). In addition, the hybrid models reduce false alarm rates, notably from 2.44% to 0.71% on BreakHis, indicating improved robustness.

These results suggest that compression-based descriptors act as practical proxies for structural organization, capturing patterns that complement semantic representations learned by deep networks. The observed improvements are therefore attributable to the structural– semantic complementarity of the proposed representation.

Despite these promising results, several limitations should be noted. The evaluation is conducted on curated datasets using lesion-centered ROIs, which may simplify the task compared to real-world clinical settings. In addition, statistical analyses are based on cross-validation folds and should be interpreted accordingly. Further validation on larger and more diverse multi-center datasets is required to assess clinical generalization.

Future work will focus on extending the framework through adaptive multi-scale modeling, multi-compressor strategies, and tighter integration of compression-based representations within neural architectures. The incorporation of automatic lesion localization and evaluation under domain shifts will also be investigated.

In summary, ACL provides a compact, interpretable, and complementary structural representation that consistently enhances deep learning models, yielding average accuracy gains of approximately +1.7%, +3.5%, and +2.0% on BUSI, CBIS-DDSM, and BreakHis, respectively, and offering a promising direction for integrating structural analysis into modern representation learning frameworks.

Funding

This research received no external funding.

Author contributions

The authors contributed equally to this work.

Conflict of interest

The authors declare no conflict of interest.

References

[1] Li M. and Vitanyi P. (2008). *An Introduction to Kolmogorov Complexity and Its Applications*, Springer, 2008.

[2] Chambon T., Guillaume J-L., Lallement J. (2023). Information Complexity Ranking: A New Method of Ranking Images by Algorithmic Complexity, *Entropy*, 25(3):439.

[3] Grunwald P.D. (2007). *The Minimum Description Length Principle*, MIT Press.

[4] Galbrun E. (2022). The minimum description length principle for pattern mining: a survey, *Data Mining and Knowledge Discovery*, 36: 1679–1727.

[5] Cilibrasi R. and Vitanyi P. (2005). Clustering by compression, *IEEE Transactions on Information Theory*, 51 (4): 1523–1545.

[6] Haralick R.M., Shanmugam K. and Dinstein I. (1973). Textural Features for Image Classification, *IEEE Transactions on Systems, Man, and Cybernetics*, 3(6): 610–621.

[7] LeCun Y., Bengio Y. & Hinton G. (2015). Deep learning, *Nature*, 521, 436–444.

[8] Bishop C.M., Bishop H. (2024). *Deep learning: foundations and concepts*, Springer.

[9] Mienye I. D., & Sun Y. (2024). A Comprehensive Review of Deep Learning: Architectures, Applications, and Trends. *Information*, 15(12), 755.

[10] Rodrigo M., Cuevas C., & García N. (2024). Comprehensive comparison between Vision Transformers and Convolutional Neural Networks for face recognition tasks. *Scientific Reports*, 14, 21392.

[11] Zhao Y., Lu J.L. (2024). Spatiotemporal Sequence Prediction Based on Spatiotemporal Self-Attention Mechanism. *International Journal of Computers Communications & Control*, 19(6), 6771.

[12] Taghanaki S.A., Abhishek K., Cohen J.P., et al. (2021). Deep Semantic Segmentation of Natural and Medical Images: A Review, *Artificial Intelligence Review*, 54: 137–178.

[13] Jiang Y., Edwards A.V., Newstead G.M. (2021). Artificial Intelligence Applied to Breast MRI for Improved Diagnosis, *Radiology*, 298(1): 38–46.

[14] Kim, K.; Lee, Y. Gray-Level Co-Occurrence Matrix Uniformity Correction Algorithm in Positron Emission Tomographic Image: A Phantom Study. Photonics. 2025; 12(1), 33.

[15] Ojala T., Pietikainen M. and Maenpaa T. (2021). Multiresolution gray-scale and rotation invariant texture classification with local binary patterns, *IEEE Transactions on Pattern Analysis and Machine Intelligence*, 24(7): 971-987.

[16] Dede A., Nunoo-Mensah H., Akowuah E.K., Boateng K.O., Adjei P.E., Acheampong F.A., et al. (2025). Wavelet-Based Feature Extraction for Efficient High-Resolution Image Classification, *Engineering Reports*, 7: e70027.

[17] Costa M., Goldberger A.L., Peng C.K. (2005). Multiscale entropy analysis of biological signals. *Physical Review E*, 71(2Pt1):021906.

[18] Ayubi, J., Chehel Amirani, M. & Valizadeh, M. (2024). A new content-aware image resizing based on Rényi entropy and deep learning, *Neural Computing & Applications*, 36, 8885–8899.

[19] Zhao Z.-Q., Zheng P., Xu S.-T., & Wu X. (2023). Object Detection with Deep Learning: A Review. *IEEE Transactions on Neural Networks and Learning Systems*, 34(8), 3949–3976.

[20] Trigka M., Dritsas E. (2025). A Comprehensive Survey of Deep Learning Approaches in Image Processing. *Sensors*, 25(2):531.

[21] He K., Zhang X., Ren S. and Sun J. (2016). Deep Residual Learning for Image Recognition, *Proceeding of 2016 IEEE Conference on Computer Vision and Pattern Recognition* (CVPR), Las Vegas, NV, USA, 2016; pp. 770–778.

[22] Huang, G., Liu, Z., Van Der Maaten, L. and Weinberger, K.Q. (2017). Densely Connected Convolutional Networks. *Proceedings of the IEEE Conference on Computer Vision and Pattern Recognition*, Honolulu, HI, USA, 2017; pp. 2261-2269.

[23] Tan M., and Le Q.V. (2019). Efficientnet: Rethinking Model Scaling for Convolutional Neural Networks. *Proceedings of the 36th International Conference on Machine Learning*, 97, 2019; pp. 6105-6114.

[24] Dosovitskiy, A. (2021). An Image Is Worth 16 × 16 Words: Transformers for Image Recognition at Scale. *Proceedings of the IEEE/CVF Conference on Computer Vision and Pattern Recognition*, New York City, 2021; pp. 45-67.

[25] Liu Z., Lin Y., Cao Y., Hu H., Wei Y., Zhang Z., et al. (2021). Swin Transformer: Hierarchical Vision Transformer Using Shifted Windows. *Proceedings of 2021 IEEE/CVF International Conference on Computer Vision (ICCV)*, Montreal, QC, Canada, 2021; pp. 9992-10002.

[26] Zhang Y., Liu T., Long M., and Jordan M. (2019). Bridging theory and algorithm for domain adaptation, *Proceedings of the 36th International Conference on Machine Learning*, pp. 7404–7413, 2019.

[27] Rudin C., (2019). Stop explaining black box machine learning models for high stakes decisions and use interpretable models instead, *Nature Machine Intelligence*, 1, 206–215.

[28] Khan, S., Naseer, M., Hayat, M., Zamir, S. W., Khan, F. S., & Shah, M. (2022) Transformers in Vision: A Survey. *ACM Computing Surveys*, 54(10).

[29] Litjens G., Kooi T., Bejnordi B.E., Setio A., Ciompi F., Ghafoorian M., et al. (2017). A survey on deep learning in medical image analysis, *Medical Image Analysis*, 42, 60-88.

[30] Hu C., Cao N., Zhou H., Guo B. (2024). Medical Image Classification with a Hybrid SSM Model Based on CNN and Transformer. *Electronics*, 13(15): 3094.

[31] Mjahed O., Mjahed S. (2026). AMoE-IDS: An Adaptive Mixture-of-Experts Framework for Cross-Dataset Intrusion Detection. *International Journal of Computers Communications & Control*, 21(4), 7480.

[32] Zenil H., Kiani N.A., Marabita F., Deng Y., Elias S., Schmidt A., et al. (2019). An Algorithmic Information Calculus for Causal Discovery and Reprogramming Systems, *iScience*, 19: 1160–1172.

[33] Hatamizadeh A., Nath V., Tang Y., Yang D., Roth H.R., Xu D. (2022). Swin UNETR: Swin Transformers for Semantic Segmentation of Brain Tumors in MRI Images. doi: 10.48550/arxiv.2201.01266

[34] Al-Dhabyani W., M. Gomaa M., Khaled H., and Fahmy A. (2020). Dataset of Breast Ultrasound Images. *Data in Brief*, 28, 104863.

[35] Lee R. S., Gimenez F., Hoogi A., Miyake K., Gorovoy M., and Rubin D. L. (2017). A Curated Mammography Data Set for Use in Computer-Aided Detection and Diagnosis Research. *Scientific Data*, 4, 170177.

[36] Spanhol F. A., Oliveira L. S., Petitjean C., and Heutte L. (2016). A Dataset for Breast Cancer Histopathological Image Classification. *IEEE Transactions on Biomedical Engineering*, 63(7): 1455–1462.

[37] Alom, M.R., Farid, F.A., Rahaman, M.A. et al. (2025). An explainable AI-driven deep neural network for accurate breast cancer detection from histopathological and ultrasound images. *Scientific Reports*, 15, 17531.

[38] Işık, G. & Paçal, İ. (2024). Few-shot classification of ultrasound breast cancer images using meta-learning algorithms. *Neural Computing and Applications*, 36(20), 12047–12059.

[39] Gheflati B. & Rivaz H. (2022). Vision transformers for classification of breast ultrasound images. *Proceedings of 44th annual international conference of the IEEE Engineering in Medicine & Biology Society* (EMBC), 2022; pp.480–483.

[40] Zhang, H. et al. (2024). Hau-net: Hybrid cnn-transformer for breast ultrasound image segmentation. *Biomedical Signal Processing and Control*, 87, 105427.

[41] Murty, P.S.R.C., Anuradha, C., Naidu, P.A. et al. (2024). Integrative hybrid deep learning for enhanced breast cancer diagnosis: leveraging the Wisconsin Breast Cancer Database and the CBIS-DDSM dataset. *Scientific Reports*, 14, 26287.

[42] El Houby E.M., Yassin N.I., (2021). Malignant and nonmalignant classification of breast lesions in mammograms using convolutional neural networks. *Biomedical Signal Processing and Control*, 70, 102954.

[43] Zahoor S., Shoaib U., Lali I.U. (2022). Breast Cancer Mammograms Classification Using Deep Neural Network and Entropy-Controlled Whale Optimization Algorithm. *Diagnostics*, 12(2): 557.

[44] Houssein E.H., Emam M.M. & Ali, A.A. (2022). An optimized deep learning architecture for breast cancer diagnosis based on improved marine predators algorithm. *Neural Computing & Applications*, 34, 18015–18033.

[45] Yamlome P., Akwaboah A. D., Marz A. & Deo M. (2020). Convolutional neural network based breast cancer histopathology image classification. *Proceedings of the 42nd Annual International Conference of the IEEE Engineering in Medicine & Biology Society* (EMBC), Montreal, QC, Canada, 2020; pp. 1144-1147.

[46] Wang G., Jia M., Zhou Q., Xu S., Zhao Y., Wang Q., et al. (2024). Multi-classification of breast cancer pathology images based on a two-stage hybrid network. *Journal of Cancer Research and Clinical Oncology*, 150(12): 505.

[47] Li X., Shen X., Zhou Y., Wang X., Li T-Q. (2020). Classification of breast cancer histopathological images using interleaved DenseNet with SENet (IDSNet). *PLoS ONE*, 15(5), e0232127.

[48] Nawaz M., Sewissy A.A., Soliman T.H.A. (2018). Multi-class breast cancer classification using deep learning convolutional neural network. *International Journal of Advanced Computer Science and Applications*, 9(6): 316–332.

Cite this paper as:

Soukaina, M.; 0uail, M. (2026). Algorithmic Compression Learning: A Hybrid Complexity–Deep Representation Framework for Medical Image Analysis, *International Journal of Computers Communications & Control*, 21(5), 7478, 2026.

https://doi.org/10.15837/ijccc.2026.5.7478